Microalgae bio-reactive façade: System thermal–biological optimization

Victor Pozzobon

Université Paris-Saclay, CentraleSupélec, Laboratoire de Génie des Procédés et Matériaux, Centre Européen de Biotechnologie et de Bioéconomie (CEBB), 3 rue des Rouges Terres 51110 Pomacle, France

ARTICLE INFO

ABSTRACT

This article explores numerically the biotechnological performances of microalgae biofaçade. The model computes the system's thermal behavior using a radiative-convective approach accounting for location on Earth and actual weather data. In a coupled manner, it simulates the microalgae culture behavior, *i.e.* light-driven growth and cell pigment content acclimation. In addition, it features refinement such as wavelength-dependent biomass optical properties and thermal-modulated biological rates. Thanks to this model, operation strategies and design possibilities were evaluated using actual weather data for a biofaçade module deployed in Marseille in 2023. Investigations revealed that a semi-batch mode of operation, while simplistic, is the most efficient way to operate a biofaçade if sole biological production is considered (about 18.0 ± 0.9 kg per year, 2.44 ± 0.12 g/L output concentration). However, if intended as an office glazing, turbidostat mode of operation should be preferred for aesthetic and visual comfort reasons (about 19.1 ± 1.1 kg per year, 0.64 ± 0.07 g/L output concentration). System optimization also confirmed the experimental observation that the system could be prone to overheating. Nevertheless, while overheating can be mitigated by increasing the reservoir thickness, this strategy is detrimental to the average output concentration. Finally, location-specific optimization revealed that a standard biofaçade module could be deployed over France, and system performances are derived for the whole country thanks to the weather forecast agency data.

1. Introduction

Since the middle of the 20th century, the human population has risen dramatically, from about 2.5 billion in 1950 to 8 billion in 2022. In parallel, the average quality of life also improved. Together, these two factors are putting our environment under evergrowing stress. Climate change, water scarcity, loss of arable lands, and biodiversity decline [1] are only a few indicators of the pressure humanity imposes. In a search to mitigate the negative impacts of these dynamics, microalgae have emerged as a potential tool to lower humanity's environmental footprint. These microorganisms can produce valuable molecules sought after by different industrial sectors (food, feed, cosmetics, and pharmaceuticals [2,3]). In addition to addressing market demands, microalgae cultivation also delivers ecosystemic services such as CO_2 fixation [4], phosphate fixation [5], nitrogen fixation [6], or effluent bioremediation [7]. Despite their potential, numerous scientific challenges must be addressed before microalgae can fully deliver on their promises. Among them, reducing the cost of microalgae production is critical.

Cutting costs can be achieved mainly in two ways for a given technological process. Either by an intensive approach, which consists of increasing the process productivity to an extent and outbeating the

costs of the associated improvements. Alternatively, an extensive approach consists of increasing the process scale to drive down production tools and process input costs. In the case of microalgal biotechnology, both can be envisioned. Nevertheless, opting for extensive outdoor cultivation offers access to large and free amounts of light, which is, most of the time, the limiting resource of a microalgae production process. Therefore, this paradigm will be explored in this work.

Deploying large-scale outdoor microalgal bioprocesses will face two challenges. First, large pieces of land would have to be acquired. Second, the culture would be submitted to natural cycles (light and temperature), complexifying process operation. Acknowledging these limitations, an idea has stemmed in scholars' and engineers' minds: integrating microalgae photobioreactors into building façades. These façade-integrated microalgae photobioreactors (in short bio-reactive façades or biofaçades) represent a possible synergy between a building and a biological system [8,9]. This association would yield benefits for the two. The photobioreactors would see their production costs reduced by taking advantage of the vertical support and utilities offered by the building (*e.g.*, water, thermal regulation), and potentially nutrients (*e.g.*, carbon dioxide reclaimed from the building). The building would gain shading, improved thermal comfort by better modulating incident

heat, pollution emission reduction, revenue stream generation, and aesthetic enhancements.

Taking a step back, microalgae biofaçade belongs to the group of advanced architectural solutions for more efficient buildings. This type of solution started to emerge with double skin façades, which allow the dynamic adjustment of solar heat gain by turning on and off natural convection in the double skin [10]. They can be further refined into production systems that manage incident sunlight and generate value out of it [11]. This is, for example, the case of a photovoltaic double skin façade, which generates electricity. Extending the benefits to carbon dioxide capture, one can mention the water façade concept (water cascading on the façade), which allows the capture of numerous pollutants and refreshes the atmosphere [12]. Yet, its operational costs are high, and the salt in the stream may deteriorate the façade. Biological façades are also means to capture carbon dioxide and create a connection to nature in urban centers. Among them, one can note microalgae biofaçade, green façades (trees integrated into the façade) [12], and biocrusts concepts (mold and lichen throwing on the façade) [9]. Microalgae biofaçade features the highest amount of positive traits, namely, producing value (green façades can also produce fruits), ease to control (trees can be managed, but biocrusts are foreseen as very hard to control), and no potential damage to the building (green façade roots can). Still, the foreseen benefits come at the cost of an increased static load on the building and additional complexity of the production system, making its optimization a difficult task.

Deciphering the entanglement between a building and a photobioreactor has been tackled with three different approaches. The first ones were experiments on a microalgae biofaçade module alone (isolated from a potential host building), which investigated basic questions such as thermal performance or biomass productivity [13–15]. Then came numerical models developments, which expanded the scope towards design questions (single vs. double glazing, façade-integrated vs. double skin) and weather impact [10,16–18,18–20] or even visual comfort and aesthetics [21,22]. Lastly, it is important to mention maybe the most significant yet short-lasting large-scale experiments that was the development of 185 m^2 of biofaçade in the BIQ house located in Hamburg, Germany, [23]. This trial delivered solid measurement of the microalgae photoconversion efficiency (4.4%, comparable to laboratory studies 5.01% [24], 5.65% [25], or 4.34% [26]), a key parameter to assess system performance. Beyond technical aspects, this field deployment also highlighted the notably positive social acceptance of the technology.

While they delivered insightful knowledge about biofaçade systems, the aforementioned studies only took the first steps on the road to cover megalopolis façades with photobioreactors. The next stages for this research initiative to turn into a large-scale reality are *in silico* biological performance assessment, system optimization, and field trial of the most promising designs. The first one was the topic of a set of companion articles, which proposed a numerical model coupling the thermal–biological aspects of the system [19,20]. In a nutshell, the model is able to predict the microalgae culture temperature by accounting for direct incident illumination from the sun, radiative heat exchange with the sky, radiative heat exchange with the surrounding and the host building, convective heat exchange with the indoor and outdoor air, and heat supplied and removed by the gas flow sparging within the culture medium. In addition, it computes illumination within the culture by coupling location on Earth (sun path model), time of the day (and the year), and weather (thanks to almost 30 years of data released by the French weather forecast agency). By coupling the former aspects, it delivers biomass production and quality (evaluated as its pigment content). Therefore, the present article intends to take biofaçade to the next step and provide a first example of location-specific purpose-driven optimization (targeting biomass production, microalgae quality, reduced module mass, ...). In addition to helping better design the microalgae biofaçade modules, this comprehensive model could

ease their operation in a model predictive control framework. Indeed, complex building-associated systems, such as microalgae biofaçade or large buildings' thermal regulation, are further complexified by the fluctuating effect of the weather. Nevertheless, Hou et al. showed that a model accounting for actual weather forecasts could be used to manage better the thermal regulation of the University of Trondheim in Norway [27]. Incidentally, their work demonstrates the applicability weather-coupled model. Finally, field trials of the most promising design would be the natural outcome of this work, yet lies outside of its scope.

The present article is structured as follows. First, the model components and capabilities are summarized. Then, bioprocess control procedures (semi-batch, turbidostat, continuous, ...) are examined in a case study. This case study is intentionally simple: city of Marseille over 2023 with a system first optimized from a thermal point of view [19]. Once the different control procedures have been analyzed, a fully coupled optimization is undergone. Indeed, as the building and the photobioreactor are in close interaction, sequential optimization is suboptimal. To lead this search for the best design (purpose-wise), Particle Swarm Optimization hybridized with a Genetic Algorithm is used [28]. Thanks to this tool, the system is optimized under different constraints (biomass production or biomass quality, thermal heat loss) to evaluate and illustrate the overall workflow capabilities. In the last part, potential for system standardization is explored by comparing two case study at two different locations (Paris versus Marseille). Finally, in order to share the tool with the community, the data and algorithms are made publicly available in an online repository.

2. System & models

2.1. Considered system

Fig. 1 presents a schematic overview of a microalgae biofaçade as well as some potential design variations. Additionally, the graphical abstract illustrates the integration of a biofaçade model into its environment. The system revolves around the reservoir containing the microalgae culture. This reservoir is enclosed by two sheets of PMMA and features a gas sparging system at its bottom. The dimensions of one biofaçade module are 1 meter in width and 4 meters in height (typical office building floor height). The thickness of the system varies based on design decisions. Moreover, the biofaçade is integrated into an office building facade at the height of approximately 20 meters above ground to ensure access to sunlight. Finally, it is positioned in the middle of the façade (as opposed to corners) to ease the description of the outdoor convective heat transfer induced by wind [29].

2.2. Thermal model

The thermal behavior model of the biofaçade is detailed, validated, and thoroughly analyzed in two companion articles [19,20]. In essence, the model calculates the evolution of the microalgae reservoir temperature by summing the contributions of absorbed and emitted convective–radiative heat fluxes (Fig. 1 - right). The considered heat fluxes include:

- incident direct sunlight, Φ_{Sun} which is divided into visible and infrared radiation,
- incident and emitted radiation towards the sky, Φ_{Sky},
- incident and emitted radiation towards the surroundings, Φ_{Sur},
- incident and emitted radiation towards the host building indoor, $\Phi_{In,Rad}$,
- convective–conductive exchange with the outdoor air, $\Phi_{Out,Conv}$,
- convective–conductive exchange with the indoor air, $\Phi_{In,Conv}$,
- heat inflow from the sparged gas, $\Phi_{Gas,Inlet}$, and heat outflow from the vented gas, $\Phi_{Gas,Outlet}$.

(a) Minimal design - Not optimized

(b) Double glazing & radiation selective film design - Optimized from a thermal point of view [19]

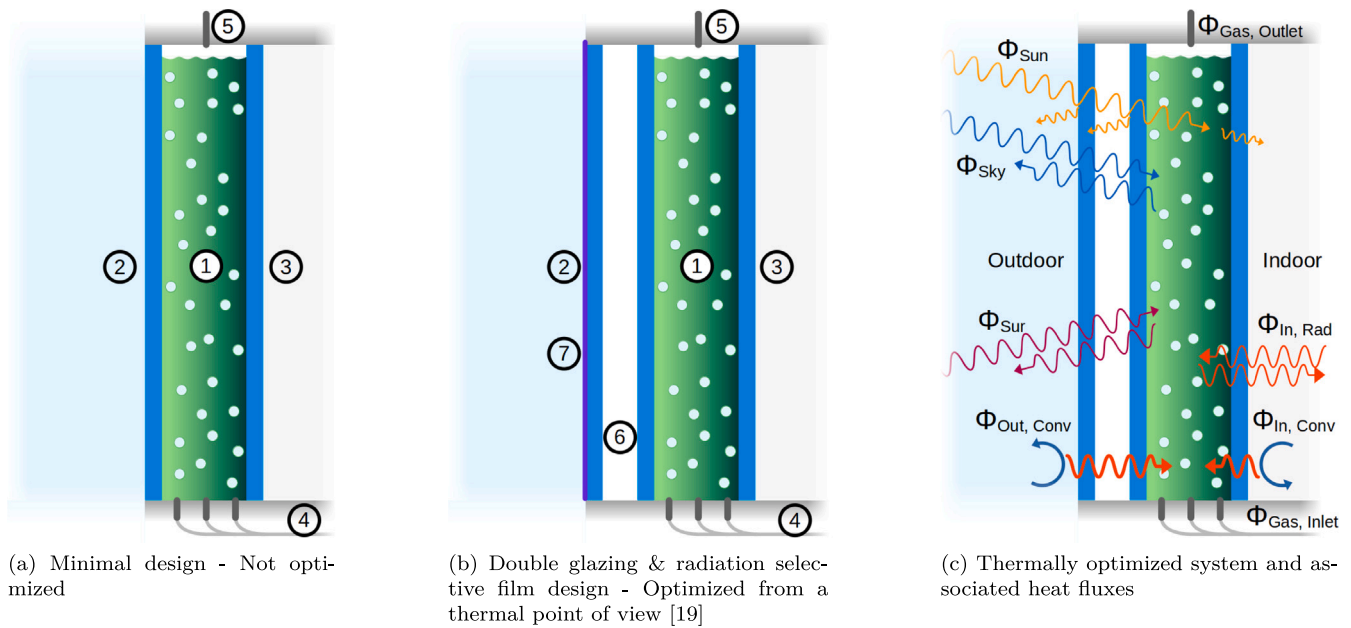(c) Thermally optimized system and associated heat fluxes

Fig. 1. Schematic representation of possible microalgae biofaçade designs. 1 - microalgae culture reservoir, 2 - outward PMMA layer, 3 - inward PMMA layer, 4 - gas sparging system, 5 - vent, 6 - double glazing, 7 - radiation-selective film. The reported heat fluxes (Φ, expressed in W/m^2) are introduced in the text.

Conductive heat fluxes within the PMMA and stagnant air layers are described using a resistance in series model. Convective exchanges are modeled based on correlations derived from experimental data (based on the wind velocity for the outside, a specific correlation for offices for the inside). Additionally, solar illumination is described using the model proposed by the Illuminating Engineering Society, which considers solar time, position on Earth, cloud cover, and orientation [30]. Radiative exchanges with the surroundings, given limited information, are modeled using the Stefan–Boltzmann formula weighted by relevant view factors and emissivities.

2.3. Actinic illumination model

Sun and sky actinic illumination are obtained from the model proposed by the Illuminating Engineering Society [30] by restricting it to the photosynthetically active radiation part of the spectrum (referred to as visible light hereinafter, for the sake of simplicity). Considerations on the absorption of light by the cultures allow to compute two key elements: the light energy absorbed by the culture, which drives cell proliferation, and the averaged level of illumination, which drives cell pigment content and photoconversion efficiency. Further refinement is added by dividing the visible spectrum into three bands: blue, green, and red. For each of them, microalgae exhibit different optical properties, based on the literature [31,32].

In order to be as faithful as possible, indoor illumination was taken into account, even though minor. The US Occupational Safety and Health Administration advises 30 foot candle in office environment [33]. Assuming a cold white spectrum for indoor lighting, it can be converted to 4.61 μmolPhoton/m^2/s in the solar spectrum (assumed to be on from 7 am to 9 pm, 5 days a week).

2.4. Biological model

The biological model used in this work is based on mass and energy balances. Cell concentration increases as a function of their ability to capture and use light efficiently. In addition to grow, the cells acclimate to the illumination conditions by manipulating their pigment content (increase under low light and the opposite under high illumination). The modulation of light absorption by the cell pigment content is also described by assuming that the absorption cross section is the product of cell pigment content and pigment intrinsic light absorption capacity [31,32]. Furthermore, cell maintenance rate is also differentiated between the day (light respiration) and night (dark respiration) [26], even though it was shown to only have a minor influence on the predictions in the companion article. Finally, cell metabolism as a whole (proliferation, maintenance, and pigment expression) is modulated by temperature [34] (subzero temperatures are never encountered). The cold temperatures slow down the different phenomena but do not damage the cells. On the contrary, the hot temperatures can harm the cells (irreversible denaturation of proteins and DNA [35]) in addition to leading to a less efficient metabolism.

In addition to its working principle, three important hypotheses underlying the model construction are to be mentioned. First, no substrate limitation (e.g., nitrogen limitation) is encountered by the culture. Second, the culture will be diluted before the cells reach a stationary phase. Third, the cells have been inoculated sufficiently in advance to avoid the appearance of a lag phase. The first two are ensured by the semi-batch, continuous, and turbidostat modes of operation, which dilute the culture by adding fresh medium. The last one is made possible by the fact that the modules operate yearlong.

2.5. Meteorological data

Meteorological data driving the model were sourced from Météo-France, the public French weather forecast agency, covering France with approximately one station per administrative region. Data range from 1996 to the present, with measurements taken every three hours. Key parameters utilized in this study include air temperature, cloud cover, wind velocity (at 10 meters above the ground), wind direction, relative humidity, and static pressure. Furthermore, the time span was reduced to the year 2023 for the sake of simplicity. Nevertheless, the reader interested in interannum variation is kindly referred to a previous article exploring the influence of weather patterns over ten years [19]. The database was last accessed in March 2024.

3. Operation strategies

Collectively, the previously introduced model components enable the determination of the culture temperature and illumination it receives. Microalgae growth can, therefore, be derived and modulated

by actual weather information. Yet, another important modulator is to be described: the bioprocess operation strategy. Still, as with any bioprocess, different manners of operating a biofaçade can be envisioned. First, two ideal cases with only one operating parameter will be considered: semi-batch and continuous. Then, a more complex and more representative of the actual operation will be investigated: the turbidostat.

3.1. Semi-batch

The semi-batch operation might be the most straightforward way to operate a biofaçade. The culture is left to grow for a given period of time. At the end of this preset duration, the biofaçade is emptied independently of the culture state. This method is modeled by replacing 95% of the reservoir volume upon reaching the preset duration. The explored interval ranges from 1 to 62 days. The chosen boundaries are obviously too low and too high to be relevant. Yet, they will help identify optimal operating conditions and associated robustness.

3.2. Continuous

A continuous mode of operation is the opposite of a semi-batch. In this mode, a value is set for microalgae concentration within the reservoir. Every time cell proliferation drives the concentration above the targeted value, a dilution is triggered with a volume adjusted to keep this concentration constant. While impractical for real-world deployment, the numerical analysis of the performances of this mode offers a valuable point of comparison. Concentrations between 0.05 and 5 g/L are investigated.

3.3. Turbidostat

A turbidostat operation appears as a technically realizable compromise between a semi-batch and a continuous strategy. From a practical point of view, it would consist of a sensor measuring the transmittance of the culture. Once a given value is reached, a dilution by a fixed preset volume is triggered. One should note that the transmittance is not the equivalent of the concentration. Indeed, by modulating their pigment content, cells can alter the reservoir transmittance without necessarily increasing their concentration. Therefore, it can be considered a proxy of cell concentration but not a measurement, strictly speaking. Therefore, this mode of operation features two parameters: the transmittance value below which a dilution is ordered and the dilution volume.

3.4. Illustration case

The different operation strategies will be illustrated using the best performing configuration identified in previous work, focusing on the thermal aspects only (summarized in Table 1) [19]. In this configuration, the biofaçade is assumed to be located in Marseille city (South of France), and the analysis will cover the whole year 2023. The two main outputs will be the produced biomass and the cell lutein content, as this carotenoid can be deemed a high-value molecule of primary interest for human health [36].

4. Optimization procedure

After discriminating the possibilities offered by the possible bioprocess control strategies on a design previously optimized from a thermal point of view, the next step is to optimize the system in a joint manner accounting for the thermal and biological aspects. Still, not all the design parameters are to be questioned. Previous investigations allowed to ascertain some decisions [19,20]. The biofaçade system will, therefore, feature double glazing, draw its gas from the building outdoors, and be oriented due South. It will not benefit from building boiler fumes injection (heat and carbon dioxide supply in winter) as

Table 1
Key geometrical, physical and bioprocess parameters describing the illustration case.

Design parameters	Reference value	Unit
Elevation of the biofaçade above the ground	20	m
Width of the biofaçade	1	m
Height of the biofaçade	4	m
Thickness of the biofaçade reservoir	0.08	m
Number of outdoor glazing	2	–
Sparged gas origin	Building	–
Use of boiler fume	Yes	–
Orientation	South	–
Strain type	*Chlorella vulgaris*	–
Radiative film type	Greenhouse	–

the required piping was deemed too expensive for too little gain. The optimized parameter will, therefore, be the reservoir thickness, the type of radiation-selective film applied on the outdoor glazing, the type of microalgae, the dilution volume, and the transmittance value below which a dilution is triggered. Table 2 summarizes the candidate space and discusses the reason and the implications of some parameter values.

4.1. Loss functions

A microalgae biofaçade system is a complex system featuring multiple outputs. Therefore, its optimization is far from straightforward [40]. Indeed, one could be willing to maximize the overall biomass production with the aim of capturing as much carbon dioxide as possible. A more refined approach could also consider the cell concentration, as handling extremely dilute culture is impractical. Going further down this line, biomass quality could also be considered, as microalgae exhibiting a high pigment content can be deemed of higher value than their pale counterparts [41]. Finally, from a building perspective, one could also wish to limit the static load and heat loss (U-value).

Therefore, four loss functions were constructed to describe the different optima. Eq. (1) aims at maximizing biomass production. Eq. (2) attempts to compromise raw biomass production and microalgae average concentration (with w_1 = 100 kg, maximal value for biomass production, and w_2 = 1 g/L). Eq. (3) includes cell quality into the procedure, with a strong focus on microalgae lutein content (with w_1 = 100 kg, w_2 = 1 g/L, and w_3 = 1 mg/g, with an average content easily reaching 5 mg/g). Furthermore, the capping on biomass production is intentional. It aims to challenge the optimization procedure further. Finally, Eq. (4) penalizes too heavy systems in a non linear manner (with w_1 = 100 kg, w_2 = 1 g/L, w_3 = 1 mg/g, and w_4 = 0.04 m).

$$f_{Loss,1} = P_{Biomass,\ kg} \tag{1}$$

$$f_{Loss,2} = P_{Biomass,\ kg}/w_1 + \overline{X_{Biomass,\ g/L}}/w_2 \tag{2}$$

$$f_{Loss,3} = P_{Biomass,\ kg}/w_1 + \overline{X_{Biomass,\ g/L}}/w_2 + \overline{Y_{Lutein,\ mg/g}}/w_3 \tag{3}$$

$$f_{Loss,4} = P_{Biomass,\ kg}/w_1 + \overline{X_{Biomass,\ g/L}}/w_2 - (L/w_4)^2 \tag{4}$$

In addition to maximizing the desired outcomes, the robustness of the operation is also of interest. The main risk is the loss of the culture because of overheating. Several options lie on the table to mitigate this risk. One could think of deployable shading, additional forced air convection using mechanical fans, or diluting the culture to limit light absorption ... As the two first solutions would require the implementation of additional systems, the third one was selected. Therefore, over a run, if the reservoir temperature approaches a temperature lethal for the cells (45.6 °C for *Chlorella vulgaris*, 45.8 °C for *Chlorella sorokiniana*), a 95% dilution is ordered to render the reservoir translucent and limit power absorption. The temperature threshold to order a dilution was chosen as the lethal temperature minus twice the standard deviation of the maximum temperature distribution over

Table 2
Candidate space for the biofaçade optimization.

Variable	Values	Comments
Radiation selective film	0	No film
	1	Greenhouse (transmittance of 26.22% for ultra-violets, 89.15% for the visible spectrum, 83.15% for the near-infrared, and 51.14% for the medium and long infrared) [37]
	2	Heat protection (transmittance of 76.4% for the visible spectrum and 42.9% for the infrared) [38]
Microalgae strain	0	Mesophilic - *Chlorella vulgaris*
		Thermophilic - *Chlorella sorokiniana*
Reservoir thickness	[2–30]	In centimeter, below 2 cm, 750 to 900 nm infrared power may pass through the water reservoir [39]
Transmittance	[0.01–0.50]	Fraction of incident green light
Dilution rate	[0.05–0.95]	Fraction of the reservoir volume replaced over a dilution

2023 (2.69 °C). Finally, if, despite this safety procedure, one of the 64 runs (used to account for uncertain parameters) reached the lethal temperature, the loss function on the candidate configuration was reduced to zero. This way, only reasonably safe configurations can be selected.

4.2. Influence of location & nation scale production potential

As the Météo-France dataset covers the whole of France, it can be used to assess for location-based differences. Therefore, the optimization procedure (Eq. (4), the one with the most constraints) was led using data describing the weather in Paris. Paris was chosen as it hosts numerous tall buildings and represents a northerner place than Marseille (less sun resource), as well as an inland location (versus coastal for Marseille, *i.e.*, less wind). From this comparison, the relevance of the conception of a standard biofaçade module is assessed, and the module production performance is computed over France. To do so, the weather conditions over the year 2023 are extracted for all the meteorological stations available in the Météo-France dataset. These data are used to predict system performance at their location before being interpolated using radial basis function (*scipy* library) over France.

4.3. Particle swarm optimizer hybridized with genetic algorithm

Once targets have been set, the question of the choice of the optimization algorithm itself has to be addressed. As the candidate space features both continuous (*e.g.*, reservoir thickness) and categorical parameters (*e.g.*, type of radiative selective film) gradient-based algorithms do not seem appropriate. On the contrary, stochastic methods have been shown to be competent to explore this type of candidate space. Among them, Particle Swarm Optimization is of note [42], as it is rather easy to implement and deploy on a parallel architecture, capable of browsing considerable candidate spaces even when described by discontinuous loss functions. To achieve all this, the Particle Swarm Optimization algorithm mimics animal group exploration patterns. In a nutshell, each particle has its own exploration trajectory (inertia parameter, modeled in its random chaotic form: inertia = $0.1r_1 + 2r_2(1-r_2)$, with r_1 and r_2 random numbers), which is modulated by information exchange with the other members of the group (social parameter, taken as 0.6) and its own history (cognitive parameter, taken as 0.6) [43]. Its versatility allows it to cover a wide range of applications from chemometrics to domestic thermal solar setup sizing [44,45]. However, its main drawback comes from the social nature of the swarm, which may mead to premature convergence into a local optimum (one particle attracting the others to it). To avoid this pitfall, Particle Swarm Optimization can be coupled with another stochastic optimization method that is naturally resistant to this type of shortcomings: Genetic Algorithms. Together, these optimization techniques form an adequate tool to solve the problem at hand [28]. The optimization algorithm parameters were set as follows: 48 particles/exemplars, and the mutation probability was set to 0.1. In addition, the maximum particle stagnation before entering a tournament was set to 15, and the tournament size

to 0.2. Runs were stopped after the swarm's best particle stagnated for 20 iterations. For a detailed practical implementation, the interested reader is referred to the following article and the freely accessible repository associated with it [44].

5. Numerical methods & uncertainty management

Previous investigations have shown that uncertainty surrounding the value of some physical parameters could have a nonnegligible impact on the thermal behavior of the system [19,20]. Notably, a global sensitivity analysis identified microalgae culture emissivity (0.8–1.0) and indoor building emissivity (0.5–0.7) as the primary drivers of variability. Additionally, the emissivity of the module surrounding (0.8–1.0) was found to act as a potential modulator. The biological parameters of the model also bear some uncertainty, namely the photoconversion efficiency (0.95–1.05 × nominal value - 4.34% -), the pigment absorption cross section (0.80–1.20 × nominal value of the wavelength-dependent chlorophyll specific absorption), and the pigment expression characteristic time (0.80–1.20 × nominal value - 8.96 h -).

To account for the effect of these uncertainties, a Monte Carlo approach was deployed. The model was executed multiple times for a given configuration, with the aforementioned parameters varied within the suggested ranges. This process generated a distribution of performance metrics from which average performances and associated standard deviations were derived. To ensure effective convergence, values were sampled using a Sobol's sequence, known for its ability to explore hypercubes uniformly and facilitate rapid and accurate convergence while minimizing computational load [46]. One could argue that such sequences tend to be conservative, treating extreme configurations as equally likely as central ones. While true, this comment also underlines that using a Sobel's sequence reinforces the robustness of the conclusions.

A convergence analysis concluded that 256 iterations were sufficient to produce stable estimates of averages and standard deviations for all the performance indicators (distribution average and standard deviation 1% and 5% stable, respectively). Therefore, this sampling was used in all cases except for the optimization. Indeed, as optimization procedures were quite long (about one week), the number of draws was reduced to 64. Even though lower, this value was deemed sufficient as it still ensured distribution average and standard deviation 1% and 10% stable, respectively.

6. Results and discussion

Results are explored in a sequential manner. First, the operation strategies (semi-batch, continuous, and turbidostat) are compared to determine the most relevant one for the illustration module design. Consequently, a turbidostat operation was retained for biofaçade design optimization. Finally, location sensitivity was assessed by comparing the best design (according to Eq. (2)) obtained in Marseille and the one in Paris, but also with interchanged locations to evaluate the generalization/standardization potential of a biofaçade design.
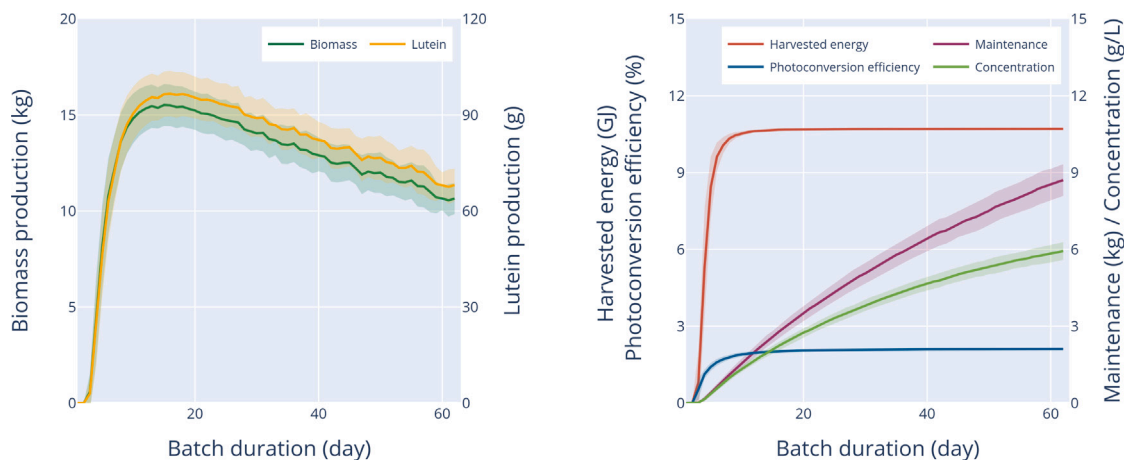
Fig. 2. Left - Biomass and lutein productions over year 2023 versus batch run duration. Right - Harvested energy, photoconversion efficiency, loss due to respiration, and average cell concentration over year 2023 versus batch run duration.

6.1. Operation strategies

6.1.1. Semi-batch

Fig. 2 (left) presents the two main performance indicators, biomass and lutein productions, for the semi-batch mode of operation. The first comment is that the two outcomes exhibit a sharp rise followed by a linear downfall. The rising part of the curves is explained by the fact that the first batch duration is one day. This timespan is obviously too short to allow a culture that was diluted by 95% to regrow fully. Consequently, the culture concentration stays near zero (Fig. 2 - right). Therefore, lengthening the batch duration improves performance by preventing the culture from being flushed away. As concentration increases, the culture harvests more and more energy, driving the overall outcome of the system. Furthermore, a darkening of the reservoir also happens as the concentration rises, allowing the photoconversion efficiency to also increase.

After this initial rise comes an inflection. This inflection originates from a competition between energy absorption, stalled as all the impinging light is absorbed, and cell respiration. Indeed, leaving the culture longer between the dilutions allows it to densify, incidentally intensifying cell maintenance. As the energy supply is limited, the overall production dwindles. In terms of figures, the maximum biomass (15.5 ± 1.1 kg) and lutein (96.7 ± 7.1 g) productions are reached for a time between dilutions of 15 and 16 days, respectively, corresponding to output concentrations of 2.10 ± 0.14 g/L and 2.24 ± 0.15 g/L. Given the observed standard deviations and differences (0.02 kg and 0.2 g, respectively), the operational optima both biomass and lutein productions can be deemed equal.

Another point is to be commented on. The kind reader surely noted that the noise level increases with the batch duration. This could have been anticipated as a 62-day batch duration corresponds to two months. Hence, only six dilutions over the year. Consequently, the time at which the culture is started has a dramatic impact. To attenuate this noise, the produced results are the average of eight simulation groups with a one-week advance in time between them (a two-month timelapse in total). Finally, even though not reported, the two other pigments described by the model (chlorophyll a and b) follow the same trend as lutein. Of course, the ratios between the different pigment contents vary to reflect photoacclimation, but the conclusions derived from lutein apply to the two others.

6.1.2. Continuous

Operating the biofaçade in continuous mode (fixed concentration) yields performances following a trend similar to the semi-batch mode of operation (Fig. 3 - left). The underlying mechanisms are the same as the semi-batch mode (Fig. 3 - right): a competition between light absorption (and usage efficiency) and maintenance (amplified by cell concentration). The maximum biomass (17.2 ± 1.1 kg) and lutein (86.7 ± 5.5 g) productions are reached for an operating concentration of 0.8 and 1.20 g/L. The difference between the two optima can be explained by the fact that a higher operating concentration induces a darker reservoir, leading to an increased the expression of lutein. Yet, at the same time, a higher operating concentration results in a higher amount of biomass lost because of respiration, hence a lower biomass production.

Overall, the results are slightly in favor of a continuous mode, compared to semi-batch, when it comes to biomass production. The performance improvement at the optimum is explained by the fact that light energy harvest and photoconversion are always near their maximum values in continuous mode, as cell concentration is always high enough to ensure a sizeable attenuation. On the contrary, in semi-batch mode, the concentration immediately following a dilution is too low to ensure the capture of all the available energy. Consequently, the maximum biomass production is slightly lower. Furthermore, it is interesting to note that the output concentrations leading to the best performances differ between the two modes. Again, it is a consequence of the dilution procedure as a time-based dilution triggering does not necessarily allow enough time for the culture to grow fully. For example, a period well-suited for the summertime will be too short during winter. Indeed, as shown in the companion article, the lower temperature over wintertime reduces culture growth rate (metabolism between 80 and 90%) compared to summer (metabolism between 90 and 100%). On the contrary, in a continuous mode of operation, this type of mismatch (growth duration versus preset batch duration) is not encountered, as regulation is tied to the cell concentration.

6.1.3. Turbidostat

Lastly, it is worth considering a turbidostat mode of operation. This mode can be considered as an easily realizable approximation of the continuous mode (in the case of a low dilution volume) or a semi-batch mode with a non-prefixed time trigger (in the case of a high dilution volume). Fig. 4 presents the biomass production and the average output concentration. Before diving into the analysis of the results, may the kind reader note that the transmission is plotted over
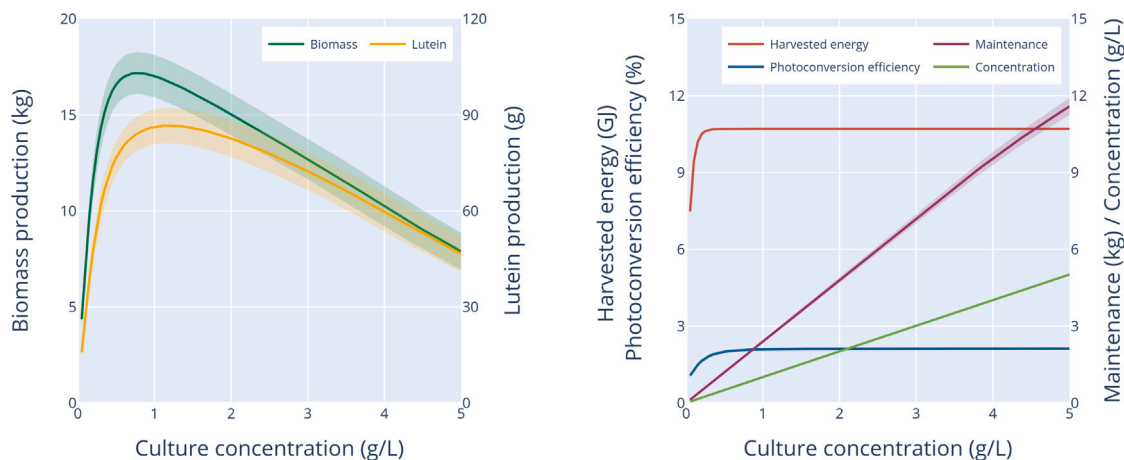
Fig. 3. Left - Biomass and lutein productions over year 2023 versus culture density in continuous mode of operation. Right - Harvested energy, photoconversion efficiency, loss due to respiration, and average cell concentration over year 2023 versus culture density.
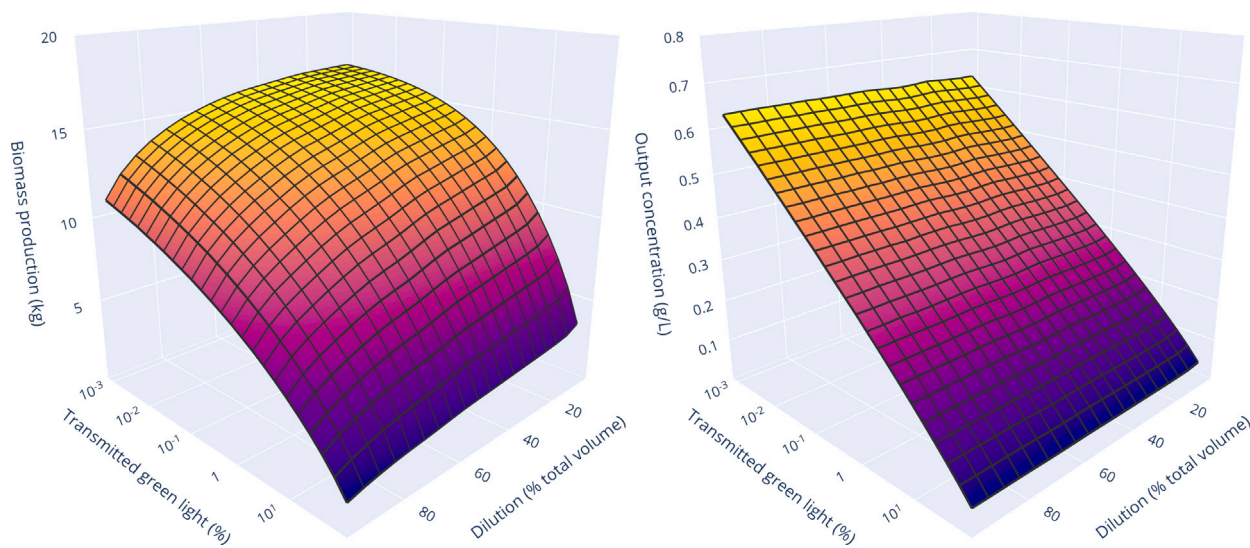
Fig. 4. Left - Biomass production over year 2023 versus turbidostat operating parameters (transmitted green light fraction and dilution volume). Right - Average output concentration over year 2023 versus turbidostat operating parameters.

a logarithmic scale. Indeed, in a turbidostat operation, the amount of light leaving the biofaçade cannot be null. Otherwise, the system would not function properly. In addition, it should also be noted operating with a transmission as low as 10^{-5} is not possible in practice (the best laboratory spectrophotometers allow absorbances of 4, hence, reaching 5 on a field device is unlikely). Yet, this configuration was explored for the sake of completeness here.

As one can see, biomass production (Fig. 4 - left) increases as transmitted light is reduced. Indeed, the culture harvests more light as the reservoir is darker, allowing a high photoconversion efficiency. The same is true, to a lesser extent, for the dilution. As the amount flushed at every dilution reduces, the biofaçade output increases. As for the semi-batch mode, it is explained by the fact that diluting by a large volume immediately induces a low cell density, preventing the culture from harnessing all the light it could. Still, those two effects plateau to reach a biomass production of 16.5 ± 1.3 kg.

It is interesting to note that this mode of operation does not feature a downward trend in productivity when operating parameters reach

excessive values. This is inherent to the way a turbidostat is designed. Indeed, the fact that some light (even though faint) has to pass through the culture forces the controller to limit the maximal concentration (Fig. 4 - right) within the reservoir. In this case, the cell concentration cannot exceed 0.65 g/L, which prevents excessive maintenance losses (driven by a too-high cell concentration).

Which is near the optimum for the system when operating in continuous mode.

6.1.4. Choice of a mode of operation

First of all, it should also be noted that all the modes of operation yield similar biomass outputs (around 16.5 kg) of microalgae of similar quality (lutein content around 5.9 mg/g). From a technical perspective, the major difference lies in the average output concentration, which is much higher hence more favorable in the case of a semi-batch operation. Furthermore, one should note that the achieved outputs are achieved thanks to high light and, incidentally, thermal energy absorption. Consequently, this leads to the appearance of relatively hot

Table 3
Best performances, pros and cons of the different modes of operation.

	Semi-batch	Continuous	Turbidostat
Produced biomass (kg)	15.5 ± 1.1	17.2 ± 1.1	16.5 ± 1.1
Average output concentration (g/L)	2.10 ± 0.14	0.80	0.63 ± 0.07
Average lutein content (mg/g)	6.21 ± 0.05	5.90 ± 0.07	5.49 ± 0.13
Pros	Simple to deploy	Constant process output	Constant process output
	High output concentration		Allow transmitted light adjustment
Cons	Low visual comfort anticipated	Complex to realize from a practical point of view	Low output concentration
	Variable module output	Opaque at optimal concentration	More expensive than semi-batch mode to implement

episodes (defined as reaching strain maximum temperature - 45.6 °C for *Chlorella vulgaris* - minus 2 °C for more than 30 min). This observation underlines the relevance of the anticipation of dangerous overheating by authors leading experimental investigation [13,17,18] and raises the question of the robustness of operation.

In addition to pure biotechnological performances, some considerations have to be drawn on the realizability of the system and its aesthetic properties. First, continuous operation based on a fixed cell concentration would be highly challenging to achieve. Second, the semi-batch mode of operation leads to highly translucent glazing (after a dilution) or opaque glazing (when the concentration overpasses 0.7 g/L). This ever-changing alternation between extrema may not foster visual comfort.

All those aspects are summarized in Table 3. As the intended use case in the context of this article is the deployment in an office environment, the turbidostat mode of operation seems to be the best-fitting one. Indeed, it ensures a tunable constant light transmission. Yet, the minimal light transmission will be adjusted to 1% (instead of 10^{-3}%) to ensure adequate illumination within the workspace (4.61 µmolPhoton/m^2/s advised by the US Occupational Safety and Health Administration [33]). Hence, 1% transmission on a sunny day allows enough light to shine into the office. Finally, if a purely productive mindset were adopted, as could be the case for the deployment in a factory, the semi-batch mode of operation would surely have been preferred as it yields a more concentrated microalgae stream and features minimalistic technological complexity to implement.

6.2. Optimal design

Based on the previous analysis, an optimal biofaçade design was carried out for a system operating in turbidostat mode. The algorithm was to optimize several outputs (Loss 1 to 4) by modulating the system reservoir thickness (2 to 30 cm), the transmitted light fraction (1 to 50%), the dilution rate (5 to 95%), the potential use of a radiation-selective film, and preferring a thermophilic strain over a mesophilic one. In addition, it was also advised to avoid any configuration resulting in dangerous overheating. The optimal system and their performances are presented in Table 4 and graphed in a relative manner in Fig. 5.

The first comment is that the optimizer is able to fulfill this assignment in all configurations. Loss function 1 maximizes biomass production at the expense of the other indicators. Loss function 2 achieves high output concentration. Loss function 3 reaches the highest cell lutein content. Loss function 4 minimizes system mass. It is also interesting to note that for all configurations, the optimizer maximizes absorbed energy by setting the transmitted fraction and the dilution rate to their lower bounds (1% and 5%, respectively). In addition, a mesophilic strain is preferred over a thermophilic one, as the warm episodes do not occur often enough to give an edge to the latter. While similarities between the optima are of interest, their discrepancies are also worst commenting.

Loss function 1 stands out by its overheating modulation strategy: very high thermal inertia (30 cm thick reservoir). Indeed, as the
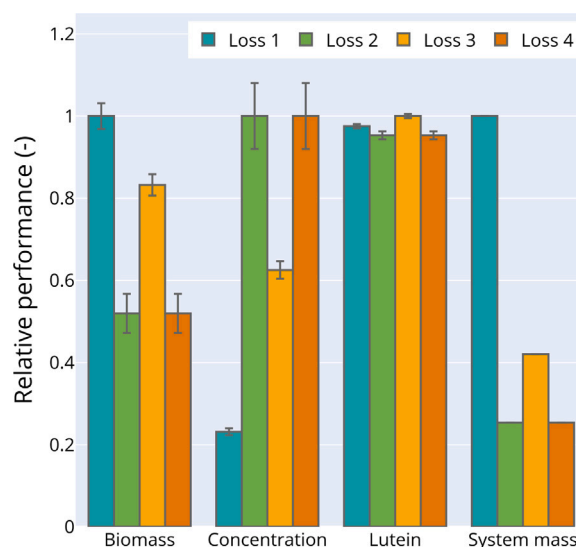
Fig. 5. Best configurations performances as a function of the applied loss function for optimization. Presented as relative to the maxima of the four configurations. Error bars - 95% confidence interval.

optimizer has no constraint to limit the system thickness, it favors high energy absorption (no radiative selection film) and temperature dampening. By deploying this strategy, the optimized system reaches good performances compared to the illustration case (16.1 ± 1.2 kg of biomass for 1% green light transmission) but low output concentration because of the large reservoir thickness. Still, it should be remembered that, as the optimizer was not allowed to select potentially hazardous configurations, the computed performances can be deemed much more robust than those in the illustration case study.

All the other loss functions (which have an incentive toward low system thickness) adopted another strategy for all systems to operate safely with a finer reservoir: applying a greenhouse radiative film. This can be explained by the fact that this film increases the relative contribution of photosynthetically active radiation over thermal radiation, hence limiting overheating without compromising biomass production. In addition to the energy harvesting strategy, the key modulations of the reservoir thickness introduced by each loss function are also worth analyzing. Loss function 2 successfully overpasses the other in terms of output concentration (about a 4-fold increase compared to loss function 1) while scarifying biomass production (about halved). On the contrary, despite a larger reservoir, loss function 3 fails to substantially increase biomass quality (assessed as microalgae lutein content). All loss functions yield biomass with similar lutein content, suggesting that biomass quality may not be easily manipulated in a biofaçade system.

Finally, it is interesting to note that loss function 4 is able to reduce the system mass (division by four) dramatically but does not find a better configuration than loss function 2. The additional incentive

Table 4
Optimal configurations and performances for the tested loss functions. Assembly mass computed as *Thickness* × 4 m *(module height)* × 1 m *(module width)* × 1000 kg/m^3 *(density of water)* + 141.6 kg (mass of the glazing). Excluding the lateral metal frame.

	Loss 1	Loss 2	Loss 3	Loss 4
Radiation selective film	None	Greenhouse	Greenhouse	Greenhouse
Microalgae strain	Mesophilic	Mesophilic	Mesophilic	Mesophilic
Reservoir thickness (cm)	30	4.9	10.5	4.9
Transmittance (–)	0.01	0.01	0.01	0.01
Dilution rate (%)	5	5	5	5
Produced biomass (kg)	15.0 ± 1.9	7.8 ± 2.9	12.5 ± 1.6	7.8 ± 2.9
Average concentration (g/L)	0.08 ± 0.01	0.34 ± 0.10	0.21 ± 0.03	0.33 ± 0.11
Average lutein content (mg/g)	4.49 ± 0.09	4.39 ± 0.18	4.60 ± 0.10	4.34 ± 0.18
Assembly mass (kg)*	1341.6	337.6	561.6	337.6
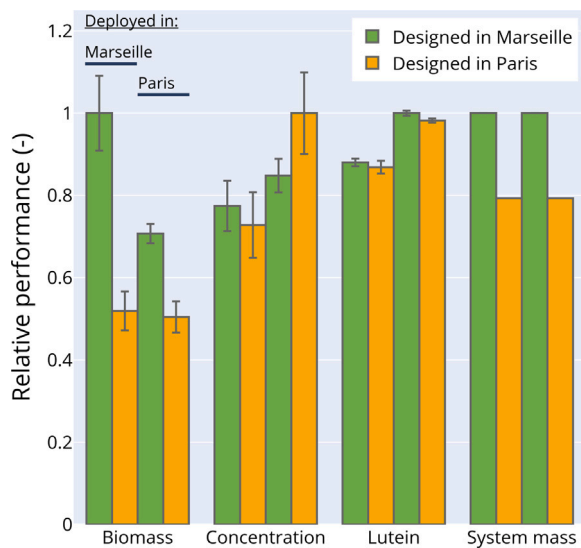
Fig. 6. Optimized configurations performances as a function of the location. M@M - Optimized for Marseille and deployed at Marseille. M@P - Optimized for Marseille and deployed at Paris. P@M - Optimized for Paris and deployed at Marseille. P@PM - Optimized for Paris and deployed at Paris. Error bars - 95% confidence interval.

toward low system mass does not allow the optimizer to reach another optimal configuration. Indeed, a strategy aiming at reducing the reservoir thickness to limit the system mass has an intrinsic limitation: overheating. Below a given thickness, the system's thermal inertia is too low to dampen incoming power surges and allow safe operation. In this regard, alternative microalgae biofaçade designs such as double skin may provide a welcome additional cooling [10,17,18] that could allow the combination of a short light path and high light absorption.

6.3. Influence of location

Finally, the influence of location (Paris versus Marseille) was investigated. To do so, the optimizer was used to derive the best configuration under Loss function 4 (optimizing biomass, concentration, and system mass) using weather data measured in Paris over 2023. Then, the cross-performance with the systems optimized in Marseille and Paris was computed. In terms of design, the only difference between the two setups is a somewhat thinner reservoir thickness in Paris (−2.0 cm) and a nonsignificantly higher dilution rate (5.4% instead of 5%).

Fig. 6 presents the relative difference between the four configurations. The first comment is that the module optimized in Marseille (larger reservoir) produces substantially more biomass than the one optimized in Paris for the two locations. Then, one can observe that the cell lutein content is not modulated by the design choices, which is

in good agreement with previous observations. Indeed, the fact that, in Paris, cell lutein content is about 10% higher than in Marseille is explained by the lower sun resource (mainly because of the could cover). Finally, module output concentration shows a nontrivial trend where both location and design come into play. A system offering a very short light path (as in Paris) placed in adequate conditions (Paris in this case) reaches a concentration 20% higher than the other possible combinations. This highlights the sensitivity of this indicator to local conditions.

From these observations, it can be concluded that biofaçade modules can be standardized with a reservoir thickness of 5 cm (close to Marseille configuration) as it limits location-specific discrepancies in terms of biomass production and output concentration. This conclusion opens the way to biofaçade module mass production and associated cost reduction. It is, therefore, possible to predict the biomass production of such a standard module for 2023 over France. Fig. 7 pictures the biomass production by the standard biofaçade module for the three trimesters of 2023. As one can see, the Mediterranean region and the Western maritime façade are the most suited places for microalgae production using a biofaçade module. On the contrary, the mountains (the Pyrenees, the Massif Central, and the Jura) and the Northern half are less productive. Using the numerical tool, it is possible to pinpoint the origin of this difference. Three hypotheses can be drawn: a substantially lower temperature in the northern regions, a lower intrinsic sun resource, or a lower effective sun resource (cloudy weather). Supplementary materials provide figures presenting the average temperature over France for the four trimesters, as well as the clear sky incident illumination, the cloud cover, and the effective sun resource. These maps show that the temperature difference across France is too low to explain the observed North-South gradient in terms of performance. In the same way, the clear sky sun resource is also homogeneous throughout France. However, the average could cover matches the discrepancies in terms of effective sun resource, itself matching the performance maps. Therefore, it can be concluded that the main meteorological phenomenon at stake behind a biofaçade system performance variability is the cloud cover and not the outdoor temperature. This conclusion clearly highlights that integrating a microalgae production system into a building dramatically reduces the production process temperature dependence, incidentally making it far more robust.

7. Conclusion

This article explored the biotechnological performances of microalgae biofaçade thanks to a numerical model describing the system's thermal and biological behavior. Operation strategies and design possibilities were evaluated using actual weather data obtained at Marseille in 2023. They revealed that a semi-batch mode of operation, while simplistic, is the most efficient way to operate a biofaçade module if sole biological production is considered. However, if intended as an office glazing, turbidostat mode of operation should be preferred
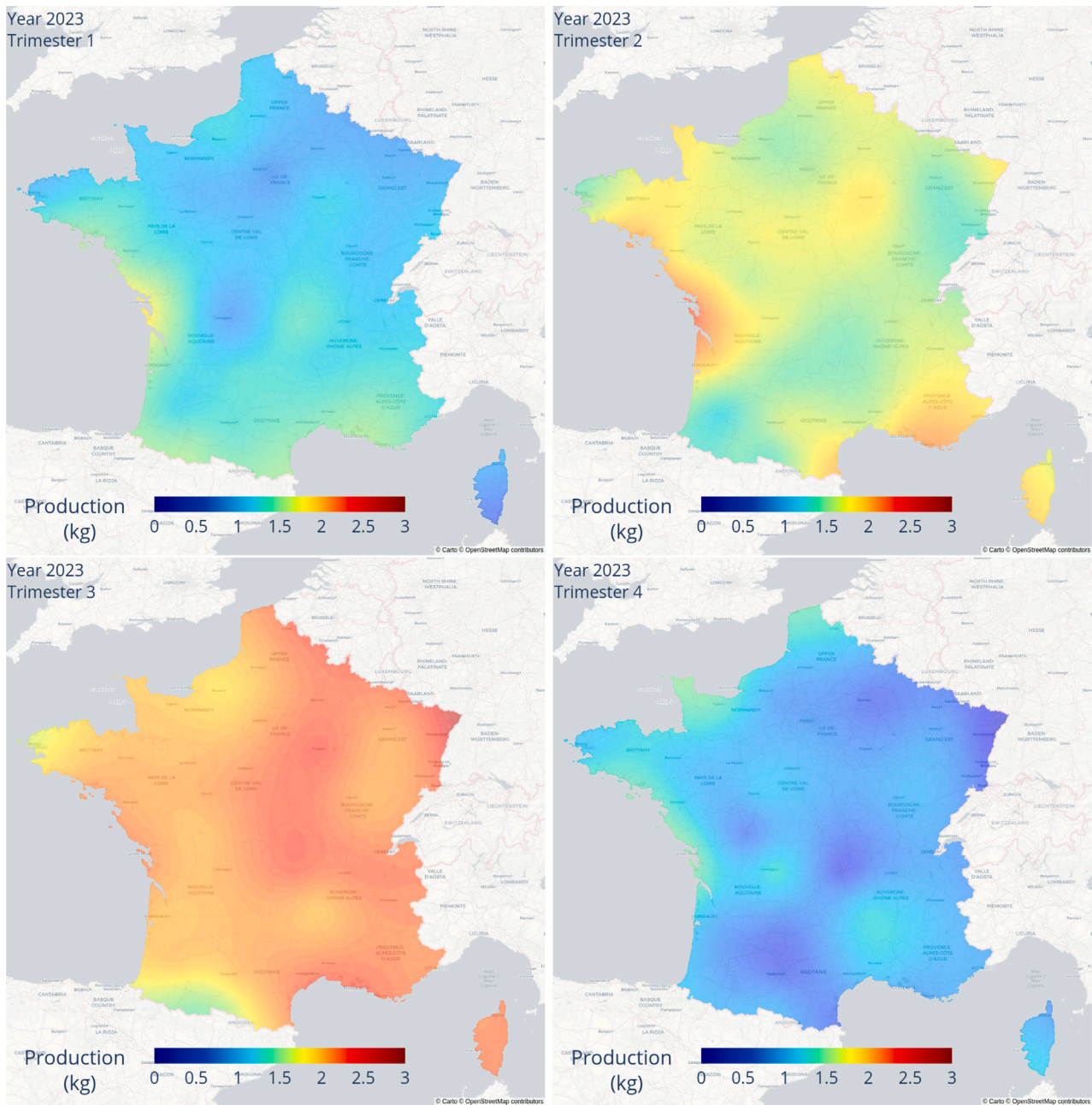
Fig. 7. Biomass production by the standard biofaçade module for the three trimester of 2023. Interpolation RBF function, *scipy* library.

for aesthetic and visual comfort reasons. System optimization also confirmed the experimental observation that the system could be prone to overheating. While it can be mitigated by increasing the reservoir thickness, this strategy is detrimental to the average output concentration. In addition, location-specific optimization revealed that a standard biofaçade module could be deployed over France. As perspectives, this work calls for its extension towards three directions: experimental validation, life cycle analysis, and national-scale implementation potential assessment.

CRediT authorship contribution statement

Victor Pozzobon: Writing – review & editing, Writing – original draft, Visualization, Validation, Supervision, Software, Resources, Project administration, Methodology, Investigation, Formal analysis, Data curation, Conceptualization.

Declaration of competing interest

The authors declare that they have no known competing financial interests or personal relationships that could have appeared to influence the work reported in this paper.

Model availability

A Python implementation of the proposed model is freely available at https://github.com/victorpozzobon/biofacade.

Acknowledgments

Appendix A. Supplementary data

Supplementary material related to this article can be found online at https://doi.org/10.1016/j.renene.2024.121377.

References

[1] S. Díaz, J. Settele, E. Brondizio, H.T. Ngo, M. Guèze, J. Agard, C. Zayas, IPBES global assessment: summary for policymakers, 2019, Retrieved from IPBES website, https://www.ipbes.net/news/ipbes-global.

[2] M. Rizwan, G. Mujtaba, S.A. Memon, K. Lee, N. Rashid, Exploring the potential of microalgae for new biotechnology applications and beyond: A review, Renew. Sustain. Energy Rev. 92 (2018) 394–404, http://dx.doi.org/10.1016/j.rser.2018.04.034, URL http://www.sciencedirect.com/science/article/pii/S1364032118302557.

[3] W. Levasseur, P. Perré, V. Pozzobon, A review of high value-added molecules production by microalgae in light of the classification, Biotech. Adv. 41 (2020) 107545, http://dx.doi.org/10.1016/j.biotechadv.2020.107545, URL http://www.sciencedirect.com/science/article/pii/S0734975020300422.

[4] H.R. Molitor, E.J. Moore, J.L. Schnoor, Maximum CO2 utilization by nutritious microalgae, ACS Sustain. Chem. Eng. 7 (10) (2019) 9474–9479, http://dx.doi.org/10.1021/acssuschemeng.9b00656.

[5] N. Brown, A. Shilton, Luxury uptake of phosphorus by microalgae in waste stabilisation ponds: current understanding and future direction, Rev. Environ. Sci. Bio/Technol. 13 (3) (2014) 321–328, http://dx.doi.org/10.1007/s11157-014-9337-3.

[6] J.A. Hellebust, I. Ahmad, Regulation of nitrogen assimilation in green microalgae, Biol. Oceanograph. 6 (3–4) (1989) 241–255, http://dx.doi.org/10.1080/01965581.1988.10749529, URL https://www.tandfonline.com/doi/abs/10.1080/01965581.1988.10749529.

[7] P.K.C. Sasi, J.M. AmbilyViswanathan, D.M. Thomas, J.P. Jacob, S.V. Paulose, Phycoremediation of paper and pulp mill effluent using Planktochlorella nurekis and Chlamydomonas reinhardtii–A comparative study, J. Environ. Treat. Techn. 8 (2) (2020) 809–817.

[8] M. Talaei, M. Mahdavinejad, R. Azari, Thermal and energy performance of algae bioreactive façades: A review, J. Build. Eng. 28 (2020) 101011, http://dx.doi.org/10.1016/j.jobe.2019.101011, URL https://www.sciencedirect.com/science/article/pii/S2352710219300841.

[9] R. Mahrous, E. Giancola, A. Osman, T. Asawa, H. Mahmoud, Review of key factors that affect the implementation of bio-receptive façades in a hot arid climate: Case study north Egypt, Build. Environ. 214 (2022) 108920, http://dx.doi.org/10.1016/j.buildenv.2022.108920, URL https://www.sciencedirect.com/science/article/pii/S0360132322001652.

[10] A.M. Elmalky, M.T. Araji, Computational fluid dynamics using finite volume method: A numerical model for Double Skin Façades with renewable energy source in cold climates, J. Build. Eng. 60 (2022) 105231, http://dx.doi.org/10.1016/j.jobe.2022.105231, URL https://www.sciencedirect.com/science/article/pii/S2352710222012372.

[11] J. Peng, L. Lu, H. Yang, An experimental study of the thermal performance of a novel photovoltaic double-skin facade in Hong Kong, Sol. Energy 97 (2013) 293–304, http://dx.doi.org/10.1016/j.solener.2013.08.031, URL https://www.sciencedirect.com/science/article/pii/S0038092X13003411.

[12] H. Rezazadeh, Z. Salahshoor, F. Ahmadi, F. Nasrollahi, Reduction of carbon dioxide by bio-façades for sustainable development of the environment, Environ. Eng. Res. 27 (2) (2022) ISBN: 1226-1025 Publisher: Korean Society of Environmental Engineers.

[13] J. Pruvost, B. Le Gouic, O. Lepine, J. Legrand, F. Le Borgne, Microalgae culture in building-integrated photobioreactors: Biomass production modelling and energetic analysis, Chem. Eng. J. 284 (2016) 850–861, http://dx.doi.org/10.1016/j.cej.2015.08.118, URL https://www.sciencedirect.com/science/article/pii/S1385894715012012.

[14] E.S. Umdu, I. Kahraman, N. Yildirim, L. Bilir, Optimization of microalgae panel bioreactor thermal transmission property for building façade applications, Energy Build. 175 (2018) 113–120, http://dx.doi.org/10.1016/j.enbuild.2018.07.027, URL https://www.sciencedirect.com/science/article/pii/S0378778817328207.

[15] C. Barajas Ferreira, L. Castro Padilla, G.V. Sánchez, A.D. González-Delgado, a.F. Barajas Solano, Design of a microalgae bio-reactive facade reactor for cultivation of Chlorella vulgaris, Contemp. Eng. Sci. 10 (22 (2017)) (2017) 1067–1074, http://dx.doi.org/10.12988/ces.2017.7884, URL http://repositorio.ufps.edu.co/handle/ufps/1617.

[16] A.M. Elmalky, M.T. Araji, Multi-objective problem of optimizing heat transfer and energy production in algal bioreactive façades, Energy 268 (2023) 126650, http://dx.doi.org/10.1016/j.energy.2023.126650, URL https://www.sciencedirect.com/science/article/pii/S0360544223000440.

[17] E. Todisco, J. Louveau, C. Thobie, E. Dechandol, L. Hervé, S. Durécu, M. Titica, J. Pruvost, A dynamic model for temperature prediction in a façade-integrated photobioreactor, Chem. Eng. Res. Des. 181 (2022) 371–383, http://dx.doi.org/10.1016/j.cherd.2022.03.017, URL https://www.sciencedirect.com/science/article/pii/S0263876222001162.

[18] F. Girard, C. Toublanc, Y. Andres, E. Dechandol, J. Pruvost, System modeling of the thermal behavior of a building equipped with facade-integrated photobioreactors: Validation and comparative analysis, Energy Build. 292 (2023) 113147, http://dx.doi.org/10.1016/j.enbuild.2023.113147, URL https://www.sciencedirect.com/science/article/pii/S0378778823003778.

[19] V. Pozzobon, Microalgae bio-reactive façade: A radiative-convective model powered by hourly illumination computation and historical weather data, J. Build. Eng. 90 (2024) 109407, http://dx.doi.org/10.1016/j.jobe.2024.109407, URL https://www.sciencedirect.com/science/article/pii/S2352710224009756.

[20] V. Pozzobon, Microalgae bio-reactive façade: Location and weather-based systematic optimization, Build. Environ. 253 (2024) 111352, http://dx.doi.org/10.1016/j.buildenv.2024.111352, URL https://www.sciencedirect.com/science/article/pii/S036013232400194X.

[21] H. Sarmadi, M. Mahdavinejad, A designerly approach to Algae-based large open office curtain wall façades to integrated visual comfort and daylight efficiency, Sol. Energy 251 (2023) 350–365, http://dx.doi.org/10.1016/j.solener.2023.01.021, URL https://www.sciencedirect.com/science/article/pii/S0038092X23000270.

[22] F. Ahmadi, S. Wilkinson, H. Rezazadeh, S. Keawsawasvong, Q. Najafi, A. Masoumi, Energy efficient glazing: A comparison of microalgae photobioreactor and Iranian Orosi window designs, Build. Environ. 233 (2023) 109942, http://dx.doi.org/10.1016/j.buildenv.2022.109942, URL https://www.sciencedirect.com/science/article/pii/S0360132322011726.

[23] J. Wurm, M. Pauli, SolarLeaf: The world's first bioreactive façade, arq: Archit. Res. Q. 20 (1) (2016) 73–79, http://dx.doi.org/10.1017/S1359135516000245, URL https://www.cambridge.org/core/journals/arq-architectural-research-quarterly/article/abs/solarleaf-the-worlds-first-bioreactive-facade/15537BF79C17E02BF6D2466C707FFB2C.

[24] I. Wagner, C. Steinweg, C. Posten, Mono- and dichromatic LED illumination leads to enhanced growth and energy conversion for high-efficiency cultivation of microalgae for application in space, Biotechnol. J. 11 (8) (2016) 1060–1071, http://dx.doi.org/10.1002/biot.201500357, URL https://onlinelibrary.wiley.com/doi/abs/10.1002/biot.201500357.

[25] R. Dillschneider, C. Steinweg, R. Rosello-Sastre, C. Posten, Biofuels from microalgae: Photoconversion efficiency during lipid accumulation, Bioresour. Technol. 142 (2013) 647–654, http://dx.doi.org/10.1016/j.biortech.2013.05.088, URL https://www.sciencedirect.com/science/article/pii/S0960852413008560.

[26] A. Oliver, C. Camarena-Bernard, J. Lagirarde, V. Pozzobon, Assessment of photosynthetic carbon capture versus carbon footprint of an industrial microalgal process, Appl. Sci. 13 (8) (2023) 5193, http://dx.doi.org/10.3390/app13085193, URL https://www.mdpi.com/2076-3417/13/8/5193.

[27] J. Hou, H. Li, N. Nord, G. Huang, Model predictive control under weather forecast uncertainty for HVAC systems in university buildings, Energy Build. 257 (2022) 111793, http://dx.doi.org/10.1016/j.enbuild.2021.111793, URL https://www.sciencedirect.com/science/article/pii/S037877882101077X.

[28] Y. Gong, J. Li, Y. Zhou, Y. Li, H.S. Chung, Y. Shi, J. Zhang, Genetic learning particle swarm optimization, IEEE Trans. Cybern. 46 (10) (2016) 2277–2290, http://dx.doi.org/10.1109/TCYB.2015.2475174.

[29] T. Defraeye, J. Carmeliet, A methodology to assess the influence of local wind conditions and building orientation on the convective heat transfer at building surfaces, Environ. Model. Softw. 25 (12) (2010) 1813–1824, http://dx.doi.org/10.1016/j.envsoft.2010.06.002, URL http://www.sciencedirect.com/science/article/pii/S1364815210001908.

[30] Recommended practice for the calculation of daylight availability, J. Illum. Eng. Soc. 13 (4) (1984) 381–392, http://dx.doi.org/10.1080/00994480.1984.10748791.

[31] R. Kandilian, A. Soulies, J. Pruvost, B. Rousseau, J. Legrand, L. Pilon, Simple method for measuring the spectral absorption cross-section of microalgae, Chem. Eng. Sci. 146 (2016) 357–368, http://dx.doi.org/10.1016/j.ces.2016.02.039, URL https://www.sciencedirect.com/science/article/pii/S0009250916300938.

[32] B. Baránková, D. Lazár, J. Nauš, A. Solovchenko, O. Gorelova, O. Baulina, G. Huber, L. Nedbal, Light absorption and scattering by high light-tolerant, fast-growing Chlorella vulgaris IPPAS C-1 cells, Algal Research 49 (2020) 101881, http://dx.doi.org/10.1016/j.algal.2020.101881, URL https://www.sciencedirect.com/science/article/pii/S2211926419310963.

[33] Code of Federal Regulations, vol. Safety and Health Regulations for Construction, no. Occupational Health and Environmental Controls, 2024.

[34] A.W. Mayo, Effects of temperature and pH on the kinetic growth of unialga Chlorella vulgaris cultures containing bacteria, Water Environ. Res. 69 (1) (1997) 64–72, http://dx.doi.org/10.2175/106143097X125191, URL https://onlinelibrary.wiley.com/doi/abs/10.2175/106143097X125191.

[35] T.D. Brock, Life at high temperatures, Science 230 (4722) (1985) 132–138, http://dx.doi.org/10.1126/science.230.4722.132, URL https://science.sciencemag.org/content/230/4722/132.

[36] C. Camarena-Bernard, V. Pozzobon, Evolving perspectives on lutein production from microalgae - a focus on productivity and heterotrophic culture, Biotech. Adv. (2024) 108375, http://dx.doi.org/10.1016/j.biotechadv.2024.108375, URL https://www.sciencedirect.com/science/article/pii/S0734975024000697.

[37] C. Balocco, L. Mercatelli, N. Azzali, M. Meucci, G. Grazzini, Experimental transmittance of polyethylene films in the solar and infrared wavelengths, Sol. Energy 165 (2018) 199–205, http://dx.doi.org/10.1016/j.solener.2018.03.011, URL https://www.sciencedirect.com/science/article/pii/S0038092X18302202.

[38] Q. Gao, X. Wu, D. Wang, Effect of fluorine and niobium co-doping on boosting the NIR blocking performance of TiO2 nanoparticles for energy efficient window, Sol. Energy 238 (2022) 60–68, http://dx.doi.org/10.1016/j.solener.2022.04.023, URL https://www.sciencedirect.com/science/article/pii/S0038092X22002717.

[39] J.A. Curcio, C.C. Petty, The near infrared absorption spectrum of liquid water, JOSA 41 (5) (1951) 302–304, http://dx.doi.org/10.1364/JOSA.41.000302, URL https://opg.optica.org/josa/abstract.cfm?uri=josa-41-5-302.

[40] N. Gunantara, A review of multi-objective optimization: Methods and its applications, in: Q. Ai (Ed.), Cogent Eng. 5 (1) (2018) 1502242, http://dx.doi.org/10.1080/23311916.2018.1502242.

[41] A. Barros, H. Pereira, J. Campos, A. Marques, J. Varela, J. Silva, Heterotrophy as a tool to overcome the long and costly autotrophic scale-up process for large scale production of microalgae, Sci. Rep. 9 (1) (2019) 13935, http://dx.doi.org/10.1038/s41598-019-50206-z, URL https://www.nature.com/articles/s41598-019-50206-z.

[42] F. Marini, B. Walczak, Particle swarm optimization (PSO). A tutorial, Chemometr. Intell. Lab. Syst. 149 (2015) 153–165, http://dx.doi.org/10.1016/j.chemolab.2015.08.020, URL http://www.sciencedirect.com/science/article/pii/S0169743915002117.

[43] R. Eberhart, J. Kennedy, A new optimizer using particle swarm theory, in: MHS'95. Proceedings of the Sixth International Symposium on Micro Machine and Human Science, 1995, pp. 39–43, http://dx.doi.org/10.1109/MHS.1995.494215, URL https://ieeexplore.ieee.org/abstract/document/494215.

[44] V. Pozzobon, W. Levasseur, C. Guerin, P. Perré, Nitrate and nitrite as mixed source of nitrogen for Chlorella vulgaris: fast nitrogen quantification using spectrophotometer and machine learning, J. Appl. Phycol. (2021) http://dx.doi.org/10.1007/s10811-021-02422-2.

[45] R. Bornatico, M. Pfeiffer, A. Witzig, L. Guzzella, Optimal sizing of a solar thermal building installation using particle swarm optimization, in: 23rd International Conference on Efficiency, Cost, Optimization, Simulation and Environmental Impact of Energy Systems, ECOS 2010, Energy 41 (1) (2012) 31–37, http://dx.doi.org/10.1016/j.energy.2011.05.026, URL https://www.sciencedirect.com/science/article/pii/S0360544211003513.

[46] I.M. Sobol, On the distribution of points in a cube and the approximate evaluation of integrals, USSR Comput. Math. Math. Phys. 7 (4) (1967) 86–112, http://dx.doi.org/10.1016/0041-5553(67)90144-9(accessedinEnglish), URL https://www.sciencedirect.com/science/article/pii/0041555367901449.